



## MODELING OF FROST BUILDUP IN LAMINAR CHANNEL FLOWS

Felipe R. de Loyola, felipeloyola@gmail.com

Christian J. L. Hermes, chermes@ufpr.br

Laboratory of Thermodynamics and Thermophysics, Department of Mechanical Engineering, Federal University of Paraná  
81531990 Curitiba-PR, Brazil

**Abstract.** *This paper advances a mathematical model based on the first-principles of mass, heat and momentum conservation to simulate the flow of moist air under frosting conditions through parallel plate channels. An evolving semi-empirical correlation is used together with a frost growth model in order to predict the frost buildup on the channel walls. The model predictions were compared with experimental data obtained elsewhere, when it was found that the predictions for the frost thickness are in good agreement with the experimental data, with all errors falling within a  $\pm 10\%$  error band. A sensitivity analysis of the key parameters that affect the frost growth and densification phenomena is also reported.*

**Keywords:** *frost formation, first-principles model, channel flow, laminar flow*

### 1. INTRODUCTION

Evaporator frosting is an undesired effect in refrigeration appliances as it decreases the evaporator capacity not only due to the insulation effect produced by the frost layer, but also because the flow passage becomes restricted, thus requiring a higher pumping power. In order to keep the internal compartment temperatures when frost takes place, the refrigeration system has to run longer, thus increasing the amount of energy required to produce the same cooling effect.

There are different kinds of evaporators adopted in refrigerating appliances, being most of them of the tube-fin type. In general, the simulation models available in the open literature for predicting frost buildup on finned-tube geometries (see Tab. 1) rely on empirical information for the frost density, which narrows the range of applicability of the model. The literature analysis also reveals that the existing models are tailored to the evaporator geometry, in such a way that there is no model available in the open literature that can handle different evaporator geometries, from plate-tube to tube-fin.

Table 1. Simulation models for predicting heat exchanger frosting

Author	Origin	Application	Approach	Validation
Kondenpudi and O'Neal (1987)	USA	Finned-tube	Global	No
Radcenco et al. (1995)	USA	No-frost	Global	No
Luer e Beer (1999)	Germany	Channel	CFD	Yes
Seker et al. (2004)	Turkey	No-frost	Global	-
Tso et al. (2006)	Singapore	Finned-tube	Distributed	-
Xia et al. (2006)	USA	Microchannel	Global	Yes
Yang et al. (2006)	South Korea	Finned-tube	Distributed	Yes
Huang et al. (2008)	Taiwan	Finned-tube	CFD	No
Lenic et al. (2009)	Croatia	Channel	CFD	Yes
Cui et al. (2011)	China	Channel	CFD	Yes
Silva et al. (2011)	Brazil	Finned-tube	Distributed	Yes
Knabben et al. (2011)	Brazil	No-Frost	Distributed	Yes

The present study is aimed at advancing, by means of a theoretical-computational approach, a generalized frost formation model that can be easily adapted to different evaporator geometries. For this purpose, a distributed one-dimensional approach was adopted together with the first-principles of mass, heat and momentum conservation in order to predict the variations experienced by the moist air that flows throughout the heat exchanger surface. The growth of the frost layer was also modelled based on a generalized semi-empirical correlation for the frost porosity in order to predict the evaporator frosting over time, thus providing the model with a larger range of applicability. The model was assessed for laminar channel flows, a simple geometry that emulates virtually any evaporator coil by changing its geometrical parameters as the heat transfer surface ( $A_s$ ), cross-section of the core ( $A_c$ ), and heat exchanger characteristics (Nu and f curves). The model predictions were compared with experimental data obtained elsewhere, when it was found that its predictions for the frost thickness agreed to the experimental data within a  $\pm 10\%$  error band.

## 2. MATHEMATICAL MODEL

### 2.1 Growth and Densification Model

In general, modeling of frost growth and densification relies on the following simplifying assumptions (Hermes et al., 2009): (i) the mass and heat transport are modeled as quasi-steady one-dimensional processes, (ii) the frost layer is uniform over the control volume, and (iii) the Lewis boundary-layer analogy is applicable, with  $Le \approx 1$ . Therefore, the frost growth and densification model is based on a mass balance within the frost layer depicted in Fig. 1, as follows:

$$\dot{m} = \frac{d}{dt} \int_0^{\delta} \rho dy \quad (1)$$

where  $\dot{m}$  is the mass flux of vapor into the porous medium. The average density of the frost layer is calculated from:

$$\rho_f = \frac{1}{\delta} \int_0^{\delta} \rho dy \approx \rho_i (1 - \varepsilon) \quad (2)$$

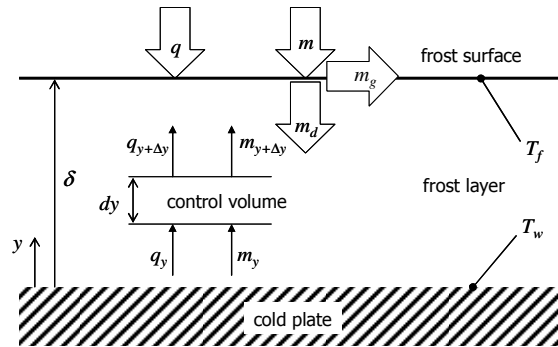


Figure 1. Physical model of growth and densification of a frost layer

Substituting eq. (1) into eq. (2), the following expression for the growth rate of the frost layer is achieved,

$$\dot{\delta} = \frac{\dot{m}/\rho_i + \delta \dot{\varepsilon}}{1 - \varepsilon} \quad (3)$$

where the term on the left-hand stands for the frost growth rate, whereas the second term on the right-hand represents the rate of frost densification. Hermes et al. (2013) showed that the frost porosity depends on the  $t^{1/2}$  scale, as follows:

$$\varepsilon = 1 - c\sqrt{t} \quad (4)$$

where  $c$  is an empirical coefficient, expressed as follows (Hermes et al., 2013):

$$c = c_0 \exp\left(c_1 \frac{i_{sv}}{c_p} \left(\frac{w_a - w_w}{T_{dew} - T_w}\right)\right) \quad (5)$$

where  $c_0=0.000448$  and  $c_1=1.663$ . Deriving eq. (5) and substituting it into (4), the thickness of the frost layer can be calculated from the following explicit 1<sup>st</sup>-order approximation:

$$\delta(t + \Delta t) \cong \delta(t) + \frac{\dot{m}/\rho_i - c\delta/2\sqrt{t}}{c\sqrt{t}} \Delta t \quad (6)$$

### 2.2 Heat and Mass Balance within the Frost Layer

The thermodynamic state at the frost surface is determined through heat and mass balances within the frost layer. Therefore, invoking the Fick and Fourier laws, the following equations can be derived for the umidity and temperature distributions within the frost layer, respectively,

$$\rho D_f \frac{d^2 w}{dy^2} = -\rho_i \dot{\epsilon} \quad (7)$$

$$k_f \frac{d^2 T}{dy^2} = i_{sv} \rho_i \dot{\epsilon} \quad (8)$$

On one hand, eq. (7) is solved considering an impermeable surface at  $y=0$ ,  $dw/dy=0$ , and a saturation condition at the frost surface,  $w=w_{sat}(T_f)$ . Equation (8), on the other hand, is solved assuming a prescribed surface temperature,  $T=T_w$ , and the heat flux continuity at the frost surface, as follows:

$$k_f \left. \frac{dT}{dy} \right|_f = q + i_{sv} \rho_i (1 - \epsilon) \dot{\delta} \quad (9)$$

where  $k_f$  is the thermal conductivity of the frost layer, calculated from  $k_f=k_{f0}+\beta\rho_f$ , with  $k_{f0}=0.131$  and  $\beta=0.0003$  (Hermes, 2012). The thermodynamic state of the moist air at the frost surface depends on the humidity ratio and the temperature. Since the former is a function of the temperature due to the saturation condition, the frost surface temperature is the only unknown. Thus, solving eq. (8), it follows that

$$T_f = T_w + \frac{q + m i_{sv}}{k_f} \delta + \frac{i_{sv} \rho_i \dot{\epsilon}}{k_f} \frac{\delta^2}{2} \quad (10)$$

Once  $T_f$  is known from eq. (10), the humidity at the frost surface can be calculated from  $w_f=w_{sat}(T_f)$ , which is used to obtain  $m$ . Since  $T_f$  depends on  $m$  in eq. (10), an iterative calculation process is adopted. Under-relaxation is required.

### 2.3 Heat and Mass Transfer on the Frost Surface

The temperature and humidity variations along the domain are obtained from energy and mass balances in the control volume depicted in Fig. 2, as follows:

$$\frac{T_k - T_f}{T_{k-1} - T_f} = \frac{w_k - w_f}{w_{k-1} - w_f} = \exp\left(-\frac{kNu}{\dot{m}c_p} \frac{A_s}{D_h}\right) \quad (11)$$

Thus, the heat and mass fluxes on the frost surface are calculated from:

$$\frac{q_k}{T_f - T_{k-1}} = \frac{m_k}{w_f - w_{k-1}} = \frac{\dot{m}c_p}{A_s} \left(1 - \exp\left(-\frac{kNu}{\dot{m}c_p} \frac{A_s}{D_h}\right)\right) \quad (12)$$

Hence, the sensible and latent heat transfer rates are calculated, respectively, from:

$$\dot{Q}_{sen} = \sum A_s q_k \quad (13)$$

$$\dot{Q}_{lat} = \sum A_s m_k i_{sv} \quad (14)$$

In addition, the frost mass accumulated over time is calculated from:

$$M(t + \Delta t) \cong M(t) + \left(\sum A_s m_k\right) \Delta t \quad (15)$$

The pressure drop is calculated from the following expression derived by Kays and London (1984):

$$\Delta p = \sum \frac{f u_c^2 \rho}{2} \frac{A_s}{A_c} \quad (16)$$

where  $u_c=u_f/\sigma$  is the air velocity at the core section, and  $\sigma=A_c/A_f$  is the free flow passage. One can note that, for laminar channel flows,  $Nu=7.541$  and  $f=24/Re$ , being both based on the hydraulic diameter,  $D_h=2H_c$ , where  $H_c=H-2\delta$  and  $A_c=H_c W$  are the height and the cross-section of the channel core.

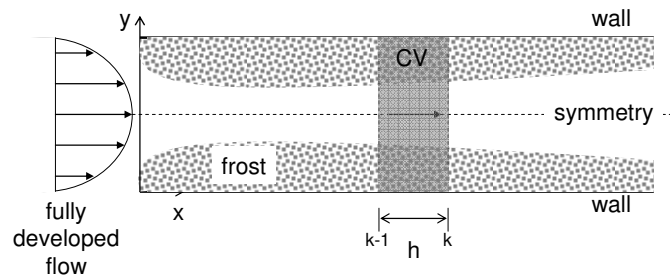


Figure 2. Schematic representation of the physical domain

### 3. MODEL VALIDATION

The model was validated against two datasets obtained elsewhere, one gathered by Hermes et al. (2009) for moist air at 16°C, 80% RH and 1 m/s flowing over a 0.1 x 0.1 m<sup>2</sup> horizontal flat plate, and another by Lenic et al. (2009) for moist air flowing at 0.6 m/s through horizontal channels with 0.048 (W) x 0.12 (L) x 0.01 (H) m<sup>3</sup>.

Figure 3 compares the model predictions for the frost thickness against the experimental data of Hermes et al. (2009) considering four different surface temperatures (-4, -8, -12 and -16°C). It can be seen that, even though this database is different than that used for obtaining the frost density correlation, the model predictions agreed quite well with the experimental data. It should be also noted that, in this case,  $Nu=0.664Re^{1/2}Pr^{1/3}$  was adopted for the sake of heat and mass transfer calculations.

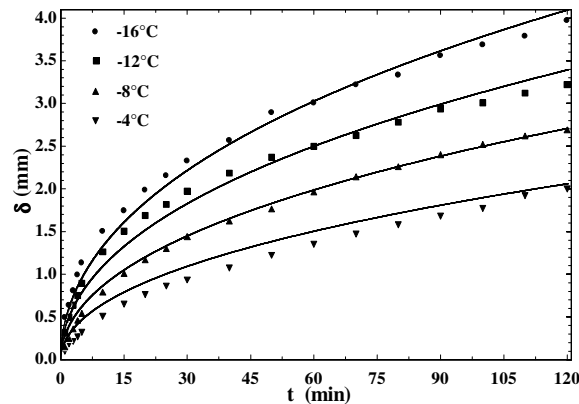


Figure 3. Comparison between model predictions and experimental data of Hermes et al. (2009)

Figure 4 compares the model predictions for the frost thickness for two experimental datapoints gathered by Lenic et al. (2009): (i) moist air at 19.8°C and 57% RH, and bottom surface at -20.5°C, and (ii) moist air at 21.4°C and 39% RH, and bottom surface at -19.5°C. The upper surface was kept thermally insulated during the experiments, in such a way that frost was formed over the bottom surface only. It can be seen in Fig. 4 that the model predictions and the experimental data agreed to within  $\pm 10\%$  error bands. In addition, the model predicted the experimental trends satisfactorily.

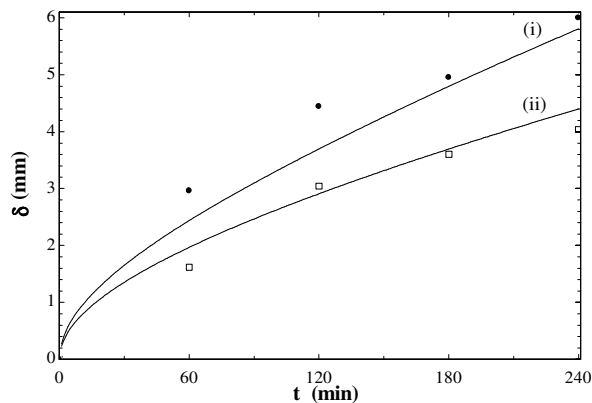


Figure 4. Comparison between model predictions and experimental data of Lenic et al. (2009)

Figure 5 explores the one-dimensional temperature profiles of the moist air (x-axis) and the frost layer (y-axis) for different times (30, 60, 120 and 240 min) for the test condition no. (ii) of Lenic et al. (2009). One can see that the frost layer is fairly uniform in the beginning (60 min), becoming uneven at the end of the simulation. As expected, the air temperature decreases along the channel, whereas the frost temperature rises from the plate to the air stream.

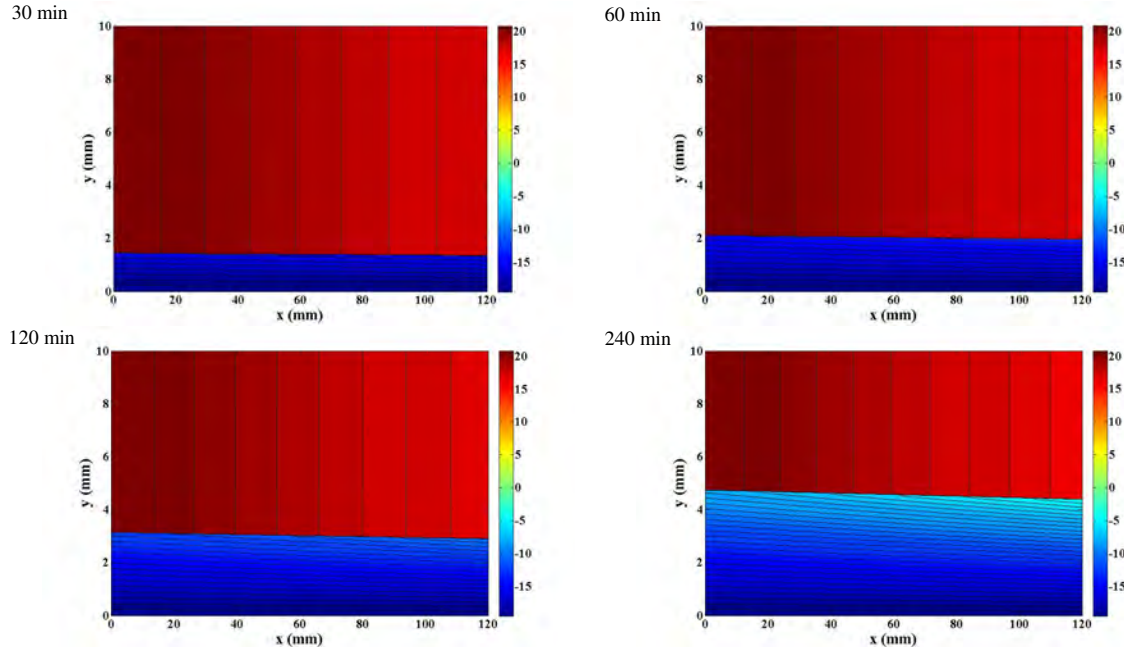


Figure 5. Temperature profiles over time for the condition no. (ii) of Lenic et al. (2009)

#### 4. SENSITIVITY ANALYSIS

The model sensitivity was assessed for two key parameters that rule the frost buildup over the channel, namely the supercooling degree and the channel spacing. The former is defined as the temperature difference between the dewpoint at the channel inlet and the surface temperature, and affects both the frost nucleation and growth processes. The latter is inversely proportional to the heat transfer coefficient, as the Nusselt number is fairly constant for laminar channel flows, thus affecting both the heat and the mass fluxes. In all cases, a 0.06 (W) x 0.04 (L) x 0.01 (H) m<sup>3</sup> channel was adopted.

##### 4.1 Supercooling degree

The supercooling degree was changed by increasing the inlet air temperature and keeping the surface temperature constrained. The behaviors of the frost thickness and density, as well as the accumulated frost mass, were evaluated for three different supercooling degrees: 8.1°C, 12.6°C and 17.3°C. Figure 6 shows that a higher supercooling degree leads to a thicker frost layer, which is mainly due to its influence on both the heat and mass fluxes. For the 17.3°C supercooling, the frost surface temperature reached 0°C, which happened after 70 min, when the simulation was stopped.

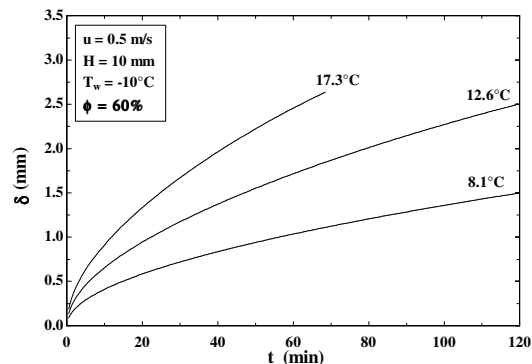


Figure 6. Time evolution of the frost thickness for various supercooling degrees

Figure 7 shows the frost density evolution over time for different supercooling degrees, where it can be seen that the higher the supercooling, higher is the density. Such an unexpected behavior can be explained by the fact that the supercooling was increased, in this exercise, by rising the airflow temperature whilst keeping both the surface temperature and the relative humidity constrained. For a constant RH, a higher airflow temperature leads to a higher absolute humidity, and so to a higher  $c$ -value in eq. (5), thus increasing the density.

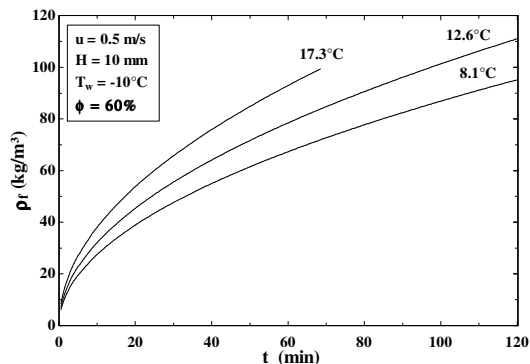


Figure 7. Time evolution of the frost density for various supercooling degrees

Figure 8 shows the accumulated frost mass along the channel over time, where one can see a fairly linear relationship between frost mass and time. This is so as  $\delta$  and  $\rho_f$  both carry the  $t^{1/2}$  scale, and since  $M \sim \delta \rho_f$ , thus  $M \sim t$ .

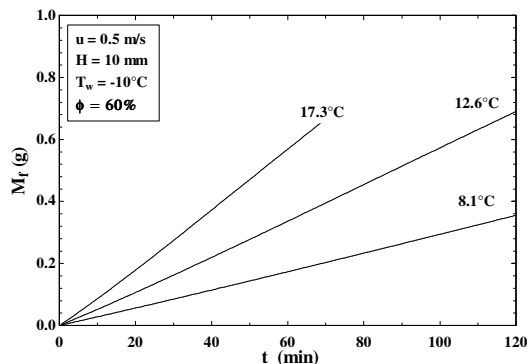


Figure 8. Time evolution of the accumulated frost mass for various supercooling degrees

#### 4.2 Channel spacing

In this analysis, the influence of channel spacing ( $H$ ) is assessed for 5, 10 and 15 mm, figures typically found in no-frost evaporators. Figure 9 shows that the frost thickness is larger the smaller the channel spacing. This is so because the smaller the channel spacing, the higher the heat transfer coefficient, and so the heat and mass fluxes, as the Nusselt number is constant in confined fully developed flows. Figure 9 also shows that a slender channel favors the frost accumulation due to the higher frost growth rate, so the channel gets rapidly clogged.

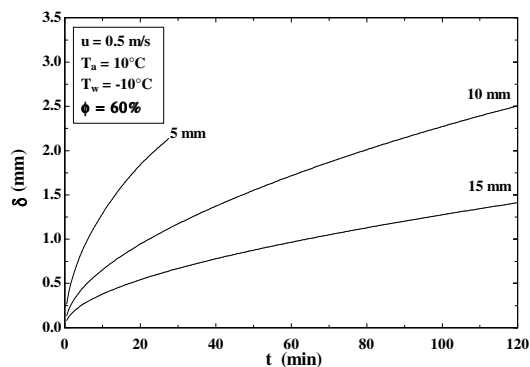


Figure 9. Time evolution of the frost density for various channel spacings

Figure 10 shows the accumulated frost mass for various channel spacings. For 5 mm, the mass accumulation rate is higher, although channels with 10 and 15 mm allow a higher amount of frost to accumulate over 120 min, as the frost growth in case of 5 mm stops after 30 min because of the frost surface temperature is above 0°C.

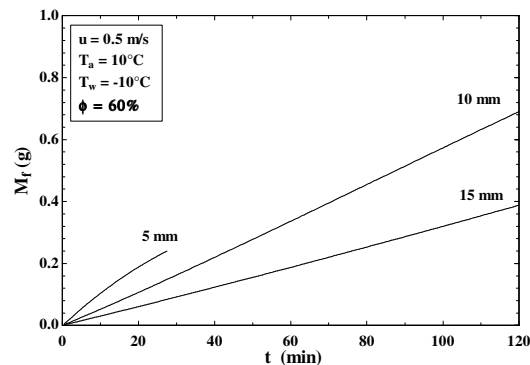


Figure 10. Time evolution of the accumulated frost mass for various channel spacings

## 5. FINAL REMARKS

A generalized mathematical model for frost buildup on complex surfaces such as plate-tube and finned-tube evaporators was put forward. The model is based on the first-principles of heat, mass and momentum conservation, being able to predict the frost growth and densification rates, as well as the evolution of the sensible and latent heat transfer rates, the pressure drop, and the blocking of the flow passage over time. The model was validated against experimental data obtained elsewhere for flat plates and channel flows, when it was observed that the numerical predictions and the experimental data agreed to within  $\pm 10\%$  error bounds.

The model sensitivity was assessed for laminar channel flows by varying both the supercooling degree and the channel spacing. The key conclusions are summarized as follows:

- A higher supercooling degree leads to a thicker frost layer, which obeys the  $t^{1/2}$  scale. In addition, the accumulated frost mass showed a fairly linear variation with time, as both  $\delta$  and  $\rho_f$  both carry the  $t^{1/2}$  scale, so that  $M \sim \delta \rho_f \sim t$ .
- The frost thickness is larger the smaller the channel spacing, as the Nusselt number is fairly constant in fully developed channel flows. Therefore, a slender channel favors the frost clogging not only due to the smaller cross-section, but also due to the higher frost growth rate.

## 6. ACKNOWLEDGMENTS

This study was carried out under the auspices of the Brazilian Government Agency CNPq (Grant No. 475886/2010-0).

## 7. REFERENCES

- Cui J, Li WZ, Liu Y, Jiang ZY, A new time- and space-dependent model for predicting frost formation, *App. Therm. Eng.* 31 (2011) 447-457
- Hermes CJL, An analytical solution to the problem of frost growth and densification on flat surfaces, *Int. J. Heat Mass Transfer* 55 (2012) 7346-7351
- Hermes CJL, Loyola FR, Nascimento VS, A dimensionless semi-empirical correlation for the density of a frost layer, 22nd Int. Congress of Mechanical Engineering, Nov. 3-7, 2013, Ribeirão Preto, SP, Brazil
- Hermes CJL, Piucco RO, Melo C, Barbosa Jr. JR, A study of frost growth and densification on flat surfaces, *Experimental Thermal and Fluid Science* 33 (2009) 371-379
- Huang JM, Msieh WC, KE XJ, Wang CC, The effects of frost thickness on the heat transfer of finned tube heat exchanger subject to the combined influence of fan types, *Applied Thermal Engineering* 28 (2008), 728-737
- Kays WM, London AL, 1984, *Compact Heat Exchangers*, McGraw-Hill, New York, USA
- Knabben FT, Hermes CJL, Melo C, In-situ study of frosting and defrosting processes in tube-fin evaporators of household refrigerating appliances, *International Journal of Refrigeration* 34 (2011) 2031-2041
- Kondenpudi S, O'Neal DL, The effects of frost growth on extended surface heat exchanger performance: A review, *ASHRAE Transactions* 93 (1987), 2.
- Lenic K, Trp A, Frankovic B, Transient two-dimensional model of frost formation on a fin-and-tube heat exchanger, *Int. J. Heat Mass Transfer* 52 (2009) 22-32

F.R. Loyola, C.J.L. Hermes  
Modeling of Frost Buildup in Laminar Channel Flows

- Luer A, Beer H, Frost deposition in a parallel plate channel under laminar flow conditions, *Int. J. Therm. Sci.* 39 (2000) 85-95
- Radcenco V, Vargas JVC, Bejan A, Lim J, Two design aspects of defrosting refrigerators, *International Journal of Refrigeration* 18 (1995), 76 - 86
- Seker D, Karatas H, Egriçan N, Frost formation on fin-and-tube heat exchangers. Part I – Modeling of frost formation on fin-and-tube heat exchangers, *International Journal of Refrigeration* 27 (2004), 367 - 374
- Silva DL, Hermes CJL, Melo C, First-Principles modelling of frost accumulation on fan-supplied tube-fin evaporators, *Applied Thermal Engineering* 31 (2011b) 2616-2621
- Tso CP, Cheng YC, Lai ACK, Dynamic behavior of a direct expansion evaporator under frosting conditions, Part I. Distributed model, *International Journal of Refrigeration* 29 (2006), 611 – 623
- Xia Y, Zhong Y, Hpnkak PS, Jacobi AM, Frost, defrost, and refrost and its impact on the air-side thermalhydraulix performance of louvered-fin, flat-tube heat exchangers, *Int. Journal of Refrigeration* 29 (2006), 1066 -1079
- Yang D, Lee K, Song S, Fin spacing optimization of a fin-tube heat exchanger under frost conditions, *Int. J. Heat Mass Transfer* 49 (2006), 2619 - 2625

## 8. NOMENCLATURE

### *Roman*

$A_c$	Cross-section of the core, $m^2$
$A_f$	Face area, $m^2$
$A_s$	Heat and mass transfer area, $m^2$
$c_p$	Air specific heat capacity at constant pressure, $J/kgK$
$D_f$	Effective diffusivity, $m^2/s$
$D_h$	Hydraulic diameter, $m$
$f$	Friction factor, dimensionless
$H$	Channel height, $m$
$h_c$	Heat transfer coefficient, $W/m^2K$
$H_c$	Channel core height, $m$
$i_{sv}$	Specific heat of desublimation, $J/kg$
$k$	Thermal conductivity, $W/mK$
$L$	Channel length, $m$
$Le$	Lewis number, dimensionless
$m$	Mass flux of moist air into the porous medium, $kg/m^2s$
$Nu$	Nusselt number, dimensionless
$p$	Pressure, $Pa$
$Pr$	Prandtl number, dimensionless
$q$	Heat flux, $W/m^2$
$\dot{Q}$	Heat transfer rate, $W$
$Re$	Reynolds number, dimensionless
$t$	Time, $s$
$T$	Temperature, $K$
$T_{dew}$	Dewpoint, $K$
$u_c$	Channel core velocity, $m/s$
$u_f$	Face velocity, $m/s$
$w$	Absolute humidity, $kg/kg$
$W$	Channel width, $m$

### *Greek*

$\delta$	Frost thickness, $m$
$\varepsilon$	Porosity, dimensionless
$\rho$	Density, $kg/m^3$
$\sigma$	Free flow passage, dimensionless

### *Subscripts*

$a$	Air
$f$	Frost
$i$	Ice
$w$	Wall